Near-Field to Near/Far-Field Transformation for Arbitrary Near-Field Geometry Utilizing an Equivalent Electric Current and MoM

Tapan Kumar Sarkar, *Fellow, IEEE*, and Ardalan Taaghol

***Abstract*—Presented here is a method for computing near- and far-field patterns of an antenna from its near-field measurements taken over an arbitrarily shaped geometry. This method utilizes near-field data to determine an equivalent electric current source over a fictitious surface which encompasses the antenna. This electric current, once determined, can be used to ascertain the near and the far field. This method demonstrates the concept of analytic continuity, i.e., once the value of the electric field is known for one region in space, from a theoretical perspective, its value for any other region can be extrapolated. It is shown that the equivalent electric current produces the correct fields in the regions in front of the antenna regardless of the geometry over which the near-field measurements are made. In this approach, the measured data need not satisfy the Nyquist sampling criteria. An electric field integral equation is developed to relate the near field to the equivalent electric current. A moment method procedure is employed to solve the integral equation by transforming it into a matrix equation. A least-squares solution via singular value decomposition is used to solve the matrix equation. Computations with both synthetic and experimental data, where the near field of several antenna configurations are measured over various geometrical surfaces, illustrate the accuracy of this method.**

***Index Terms*—Antenna arrays.**

I. Introduction

THERE exists a large volume of literature on near-field to far-field transformation [1]–[3]. Presented here is a method for near-field to near/far-field transformation which requires no specific geometry for near-field measurements. The earliest work in this area was performed in the early sixties by Brown and Jull [4] for two-dimensional (2-D) cylindrical scanning in which the radiated field was expanded in terms of a series of radially expanding modes. The amplitude and phase of each mode were calculated by a Fourier analysis of the measured near field and the radiation pattern was obtained as a Fourier series containing those measured amplitudes and phases. Kerns [5] also did work on planar scanning. Probe-compensated spherical scanning formulas were developed by Jenson [6] in 1970. Wacker proposed a method to extract the modal coefficients from spherical near-field measurements and a scheme to use fast Fourier transform (FFT) to compute those coefficients [7], [8]. Leach and Paris [9] extended the 2-D cylindrical scanning theory to three dimensions in the early seventies. This method is derived by first expanding both the field radiated by the antenna and the field radiated by the measurement probe, when it is used as a transmitter, into cylindrical wave expansions. An overview of the development of near-field scanning techniques is found in [10] where the theory of near-field antenna measurements is outlined beginning with ideal probes scanning on arbitrary surfaces and ending with arbitrary probes scanning on planar, cylindrical, and spherical surfaces. Appel–Hansen presents a detailed description of planar, cylindrical, and spherical scanning in [11]. Narasiman and Kumar [12] have tried an approach in which near fields on a planar surface are used to synthesize source currents on planar arrays or apertures. This technique makes use of an exact solution to the fields radiated by the aperture antenna without disregarding the source currents. The far-fields represent the Fourier transform of the near field, which extend throughout all space. However, this only provides the true fields in the region $z \geq 0$ in terms of the finite Fourier transform of the measured near fields over a planar surface.

In this approach, by using the equivalence principle [13], an equivalent electric current replaces the radiating antenna. Furthermore, it is assumed that the near field is produced by the equivalent electric current and, therefore, via Maxwell's equation from the measured near-field data, the current source can be determined. Once this is accomplished, the near field and the far field of the radiating antenna in all regions in space in front of the radiating antenna can be determined directly from the equivalent electric current. It is consequently shown that from the knowledge of the field in one region of space measured over any geometry, the field values for any other region can be extrapolated, therefore confirming the concept of analytic continuity.

An electric field integral equation is developed which pertains to the measured near fields and the equivalent electric current. This integral equation has been solved for the unknown electric current source through a moment method procedure [14] with point matching, where the equivalent current is expanded as linear combinations of 2-D pulse-basis functions and, therefore, the integral equation is then transformed into a matrix equation. In general, the matrix is rectangular whose dimensions depend on the number of field and source points chosen. The matrix equation is solved by the moment matrix, which is decomposed into a set of orthogonal matrices. The set of orthogonal matrices can easily be inverted.

Manuscript received April 14, 1997; revised August 1, 1998.

The authors are with the Department of Electrical and Computer Engineering, Syracuse University, Syracuse, NY 13244 USA.

Publisher Item Identifier S 0018-926X(99)04436-1.

Another aspect of this approach is that the numerical integrations in the process of creating the moment matrix elements have been avoided by taking a limiting case. Since the field points and the source points are to never coincide and if their distances are much larger than the sizes of the current patches, then the pulse-basis functions expanding the current source can be approximated by the Hertzian dipoles.

The formulation and the theoretical basis for the equivalent electric current approach along with the formation of the corresponding matrix equation using the method of moments and its solution using the method of least squares via singular value decomposition is presented in the following sections.

Near-field to far-field transformations are generally used for the far-field characterization of electrically large arrays and particularly phased arrays. The near-field measurement of a large antenna is not only very time consuming, but cumbersome because of measuring the fields over certain large canonical surfaces with high spatial accuracy. What this method provides is a methodology not only to minimize the number of measured data samples that needs to be collected from a measurement but also shows that it is not necessary to compute the fields over an entire canonical surface-imagine measuring over a cylindrical/spherical near-field measurement to deal with a 10-m-long antenna with submillimeter spatial accuracy! For planar near-field to far-field measurements, the method presented in this paper may be more efficient and accurate than conventional techniques as documented in the various references [17]–[21]. Also, in this method, the measured field points need not satisfy the Nyquist sampling criteria. Hence, this paper is quite suitable for pattern measurements of large phased arrays.

II. Formulation of the Electric Field Integral Equation by the Equivalent Electric Current Approach and MoM

Consider an arbitrary-shaped antenna, as shown in Fig. 1, which radiates into free-space. The aperture of the antenna is in a surface which separates all space into left-half and right-half spaces. The aperture of the antenna is placed in the xy plane and is facing the positive z axis. Since we are interested only in the electromagnetic field in the region where $z > 0$, we place a perfect magnetic conductor in front of the radiating antenna extending to infinity in the x and y directions on the xy plane of the antenna. This is denoted by S_∞. By the equivalence principle [13], a surface electric current $\mathbf{J}'$ can be placed on a perfect magnetic conductor covering the aperture of the antenna. The value of $\mathbf{J}'$ is equal to the tangential value of the magnetic field on the xy-plane (Fig. 1)

$$\mathbf{J}' = \hat{n} \times \mathbf{H} \quad \text{on } S_\infty \tag{1}$$

where $\mathbf{H}$ is the magnetic field on the xy plane and $\hat{n}$ is the unit outward normal to the xy plane, pointing in the direction of the positive z axis.

Using image theory [13], an electric current $\mathbf{J}$ may be introduced on the xy plane whose value is

$$\mathbf{J} = 2\mathbf{J}'. \tag{2}$$

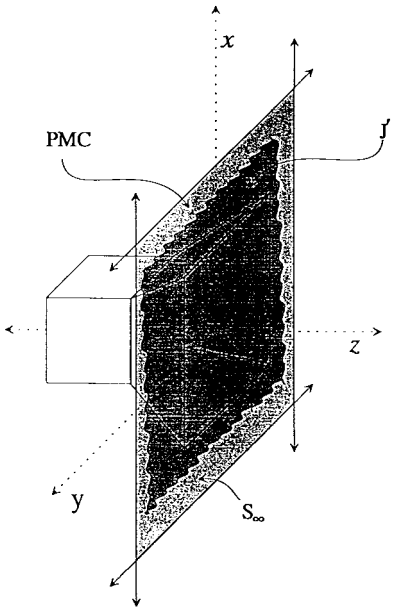

Fig. 1. Equivalent problem with an electric current sheet.

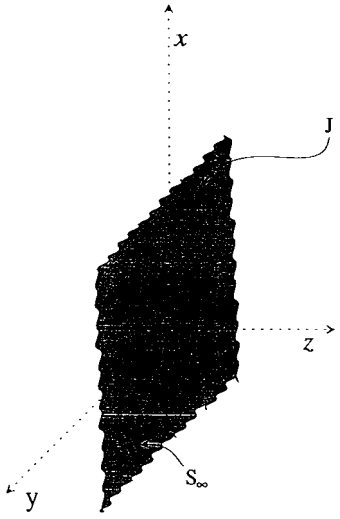

Fig. 2. Equivalent electric current sheet radiating in free-space.

Therefore,

$$\mathbf{J}' = 2\hat{n} \times \mathbf{H} \tag{3}$$

radiating in free-space (Fig. 2) and producing exactly the same field as the original antenna in the region $z \geq 0$. Now the measured electric near field may be used to determine $\mathbf{J}$ from

$$\mathbf{E}_{\text{meas}} = \mathbf{E}(\mathbf{J}) \tag{4}$$

where $\mathbf{E}_{\text{meas}}$ is the electric near field measured over a geometry at a distance away from the aperture of the radiating antenna.

From Maxwell's equations, the electric field operator is expressed in terms of its electric current source in a homogeneous medium as

$$\mathbf{E}(\mathbf{J}) = -j\omega\mu\mathbf{A}(\mathbf{J}) + \frac{1}{j\omega\varepsilon}\nabla(\nabla \cdot \mathbf{A}(\mathbf{J})) \tag{5}$$

where $\mathbf{A}(\mathbf{J})$ is the magnetic vector potential defined as

$$\mathbf{A}(\mathbf{J}) = \frac{1}{4\pi} \int_{S_\infty} \mathbf{J}(\mathbf{r}') g(\mathbf{r}, r')\, ds' \tag{6}$$

where

$$\nabla = \frac{\partial}{\partial x}\hat{x} + \frac{\partial}{\partial y}\hat{y} + \frac{\partial}{\partial z}\hat{z} \tag{7}$$

and

$$g(\mathbf{r}, \mathbf{r}') = \frac{e^{-jk_0|r-r'|}}{|\mathbf{r}-\mathbf{r}'|} = \frac{e^{-jk_0 R}}{R}. \tag{8}$$

The primed variables correspond to the source values and the unprimed variables correspond to the field values. The region S_0 where the equivalent electric current resides is taken to be a rectangle in the xy plane for which $-w_x/2 \le x \le w_x/2$ and $-w_y/2 \le y \le w_y/2$. S_0 is divided into $N_x N_y$ equally spaced rectangular patches with dimensions Δx and Δy (Fig. 3) given by

$$\Delta x = w_x/N_x \tag{9}$$

$$\Delta y = w_y/N_y \tag{10}$$

x_i and y_j are the x and y coordinates of the center of the ijth patch and are given by

$$x_i = -w_x/2 - \Delta x/2 + i\Delta x \tag{11a}$$

$$y_j = -w_y/2 - \Delta y/2 + j\Delta y. \tag{11b}$$

The components of the equivalent electric current J_x and J_y are approximated by equally spaced 2-D pulse basis functions

$$J_x(x', y') = \sum_{i=1}^{N_x}\sum_{j=1}^{N_y} \gamma_{ij}\Pi_{ij}(x', y') \tag{12a}$$

$$J_y(x', y') = \sum_{i=1}^{N_x},\sum_{j=1}^{N_y} \mathrm{B}_{ij}\Pi_{ij}(x', y') \tag{12b}$$

where γ_{ij} and B_{ij} are the unknown coefficients of the x- and y-directed electric currents, respectively, on the ijth patch. $\prod_{ij}(x', y')$ is the 2-D pulse basis function pertaining to the ijth patch and is defined as

$$\prod_{ij}(x', y') = \begin{cases} 1, & \text{if } \begin{cases} x_i - \dfrac{\Delta x}{2} \le x' \le x_i + \dfrac{\Delta x}{2} \\ y_j - \dfrac{\Delta y}{2} \le y' \le y_j + \dfrac{\Delta y}{2} \end{cases} \\ 0, & \text{otherwise.} \end{cases} \tag{13}$$

Since it is assumed that the measured field points are far from the current carrying region S_0, the 2-D pulse-basis function may be approximated by a Hertzian dipole existing at the center of the ijth patch. Therefore

$$\Pi_{ij}(x', y') \approx \Delta x \Delta y \delta(x' - x_i, y' - y_j). \tag{14}$$

When (14) is substituted into (12) we have

$$J_x(x', y') = \sum_{i=1}^{N_x}\sum_{j=1}^{N_y} \gamma_{ij}\Delta x\Delta y\delta(x' - x_i, y' - y_j) \tag{15a}$$

$$J_y(x', y') = \sum_{i=1}^{M},\sum_{j=1}^{N} \mathrm{B}_{ij}\Delta x\Delta y\delta(x' - x_i, y' - y_j). \tag{15b}$$

The effect of the δ functions in (15) is to replace the integrals in (19) by their integrands evaluated at the positions of the δ functions.

Since the electric near-field is known at discrete points on the geometry over which it has been measured, a point-matching procedure [14] is chosen. Substituting (15) into (4) and (5) and utilizing point matching, the following matrix equation is obtained:

$$\begin{bmatrix} \vec{E}_{\mathrm{meas},\,\theta} \\ \vec{E}_{\mathrm{meas},\,\phi} \end{bmatrix} = \begin{bmatrix} L_{11} & L_{12} \\ L_{21} & L_{22} \end{bmatrix} \begin{bmatrix} \vec{J}_x \\ \vec{J}_y \end{bmatrix} \tag{16}$$

where $\vec{E}_{\mathrm{meas},\,\theta}$ and $\vec{E}_{\mathrm{meas},\,\phi}$ are complex quantities whose elements are the θ and ϕ components of the electric near field, respectively, measured at discrete points. $\vec{J}_x$ and $\vec{J}_y$ are column vectors whose elements are the unknown coefficients γ_{ij} and B_{ij}, respectively. L_{11}, L_{12}, L_{21}, and L_{22} are the submatrices of the entire moment matrix in (16) whose explicit expressions are given in (17a)–(17d)

$$\begin{aligned}
&[L_{11}]_{k,\ell} \\
&= \Bigg[\cos\theta_k \cos\phi_k\, e^{-jk_0 R_{k,\ell}} \\
&\quad \cdot \Bigg[(x_k^f - x_\ell)^s \left(\frac{j\omega\mu}{R_{k,\ell}^3} + \frac{3\eta}{R_{k,\ell}^4} + \frac{3}{j\omega\varepsilon R_{k,\ell}^5}\right) \\
&\quad - \left(\frac{j\omega\mu}{R_{k,\ell}} + \frac{\eta}{R_{k,\ell}^2} + \frac{3}{j\omega\varepsilon R_{k,\ell}^3}\right)\Bigg] \\
&\quad + \cos\theta_k \sin\phi_k\, e^{-jk_0 R_{k,\ell}} \\
&\quad \cdot \left[(x_k^f - x_\ell^s)(y_k^f - y_\ell^s)\left(\frac{j\omega\mu}{R_{k,\ell}^3} + \frac{3\eta}{R_{k,\ell}^4} + \frac{3}{j\omega\varepsilon R_{k,\ell}^5}\right)\right] \\
&\quad - \sin\theta_k\, e^{-jk_0 R_{k,\ell}} \\
&\quad \cdot \left[(x_k^f - x_\ell^s)(z_k^f)\left(\frac{j\omega\mu}{R_{k,\ell}^3} + \frac{3\eta}{R_{k,\ell}^4} + \frac{3}{j\omega\varepsilon R_{k,\ell}}\right)\right]\Bigg] \\
&\quad \cdot \frac{\Delta x\Delta y}{4\pi}
\end{aligned} \tag{17a}$$

$$\begin{aligned}
&[L_{12}]_{k,\ell} \\
&= \Bigg[\cos\theta_k \cos\phi_k\, e^{-jk_0 R_{k,\ell}} \\
&\quad \cdot \left[(x_k^f - x_\ell^s)(y_k^f - y_\ell^s)\left(\frac{j\omega\mu}{R_{k,\ell}^3} + \frac{3\eta}{R_{k,\ell}^4} + \frac{3}{j\omega\varepsilon R_{k,\ell}^5}\right)\right] \\
&\quad + \cos\theta_k \sin\phi_k\, e^{-jk_0 R_{k,\ell}} \\
&\quad \cdot \Bigg[(y_k^f - y_\ell^s)^2 \left(\frac{j\omega\mu}{R_{k,\ell}^3} + \frac{3\eta}{R_{k,\ell}^4} + \frac{3}{j\omega\varepsilon R_{k,\ell}^5}\right) \\
&\quad - \left(\frac{j\omega\mu}{R_{k,\ell}} + \frac{\eta}{R_{k,\ell}^2} + \frac{1}{j\omega\varepsilon R_{k,\ell}^3}\right)\Bigg] \\
&\quad - \sin\theta_k\, e^{-jk_0 R_{k,\ell}} \\
&\quad \cdot \left[(y_k^f - y_\ell^s)(z_k^f)\left(\frac{j\omega\mu}{R_{k,\ell}^3} + \frac{3\eta}{R_{k,\ell}^4} + \frac{3}{j\omega\varepsilon R_{k,\ell}^5}\right)\right]\Bigg] \\
&\quad \cdot \frac{\Delta x\Delta y}{4\pi}
\end{aligned} \tag{17b}$$

$$
\begin{aligned}
&[L_{21}]_{k,\ell} \\
&\quad = \Bigg[-\sin\phi_k\, e^{-jk_0 R_{k,\ell}} \\
&\qquad \cdot \Bigg[(x_k^f - x_\ell^s)^2 \left(\frac{j\omega\mu}{R_{k,\ell}^3} + \frac{3\eta}{R_{k,\ell}^4} + \frac{3}{j\omega\varepsilon R_{k,\ell}^5} \right) \\
&\qquad - \left(\frac{j\omega\mu}{R_{k,\ell}} + \frac{\eta}{R_{k,\ell}^2} + \frac{3}{j\omega\varepsilon R_{k,\ell}^3} \right) \Bigg] \\
&\qquad - \cos\phi_k\, e^{-jk_0 R_{k,\ell}} \\
&\qquad \cdot \left[(x_k^f - x_\ell^s)(y_k^f - y_\ell^s) \left(\frac{j\omega\mu}{R_{k,\ell}^3} + \frac{3\mu}{R_{k,\ell}^4} + \frac{3}{j\omega\varepsilon R_{k,\ell}} \right) \right] \Bigg] \\
&\qquad \cdot \frac{\Delta x \Delta y}{4\pi}
\end{aligned}
\tag{17c}
$$

$$
\begin{aligned}
&[L_{22}]_{k,\ell} \\
&\quad = \Bigg[-\sin\phi_k\, e^{-jk_0 R_{k,\ell}} \\
&\qquad \cdot \Bigg[\left[(x_k^f - x_\ell^s)(y_k^f - y_\ell^s) \left(\frac{j\omega\mu}{R_{k,\ell}^3} + \frac{3\eta}{R_{k,\ell}^4} + \frac{3}{j\omega\varepsilon R_{k,\ell}^5} \right) \right] \\
&\qquad + \cos\phi_k\, e^{-jk_0 R_{k,\ell}} \\
&\qquad \cdot \left[(y_k^f - y_\ell^s)^2 \left(\frac{j\omega\mu}{R_{k,\ell}^3} + \frac{3\mu}{R_{k,\ell}^4} + \frac{3}{j\omega\varepsilon R_{k,\ell}^5} \right) \right. \\
&\qquad \left. - \left(\frac{j\omega\mu}{R_{k,\ell}} + \frac{\mu}{R_{k,\ell}^2} + \frac{1}{j\omega\varepsilon R_{k,\ell}^3} \right) \right] \Bigg] \Bigg] \\
&\qquad \cdot \frac{\Delta x \Delta y}{4\pi}
\end{aligned}
\tag{17d}
$$

where θ_k and ϕ_k are the θ and ϕ coordinates, respectively, of the kth-field measuring point and x_ℓ^s and y_ℓ^s are the x and y coordinates, respectively, of the ℓth source point. $R_{k,\ell}$ is the distance between the kth field point and the ℓth source point and is given by

$$
R_{k,\ell} = \sqrt{(x_k^f - x_\ell^s)^2 + (y_k^f - y_\ell^s)^2 + (z_k^f)^2}. \tag{18}
$$

Note that in (17) the two subscripts i and j have been replaced by the single subscript ℓ. That is (x_ℓ^s, y_ℓ^s) is (x_i, y_j) where i and j are determined by ℓ.

The resulting matrix equation (16) with supporting equation (17) has been solved for the elements $\vec{J}_x$ and $\vec{J}_y$. This matrix equation is solved using the method of least squares with singular value decomposition [15].

Let us rewrite (16) in the following form:

$$
\mathbf{A}\vec{X} = \vec{\mathbf{E}}. \tag{19}
$$

In (19), $\mathbf{A}$ is the moment matrix and in general is rectangular with dimensions $M \times N$, where M is the number of θ and ϕ components of the measured electric field (i.e., M is the number of equations) and N is twice the number of patches in Fig. 3 (i.e., N is the total number of unknowns). $\vec{X}$ is the $N \times 1$ unknown column vector of the elements $\vec{J}_x$ and $\vec{J}_y$, and $\vec{E}$ is the right-hand side or the known $M \times 1$ column vector containing the measured values of electric field.

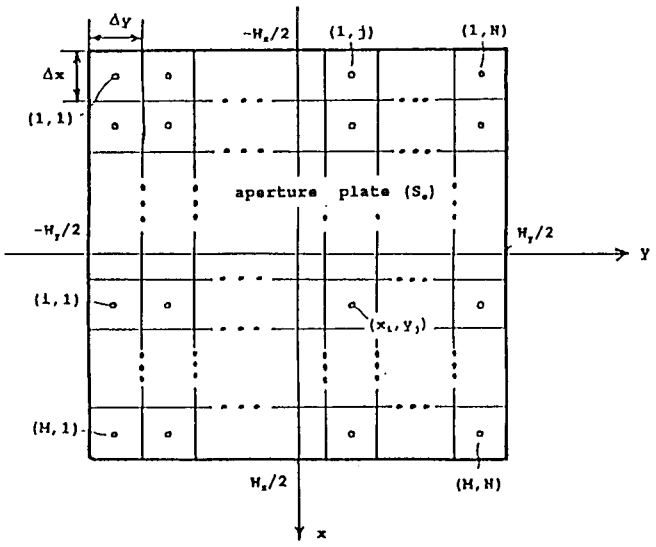

Fig. 3. Plate S_o on the xy plane where the equivalent electric current resides.

Using singular value decomposition, the matrix $\mathbf{A}$ can be decomposed into

$$
\mathbf{A} \approx \mathbf{U}\Sigma\mathbf{V}^H \tag{20}
$$

where the matrix $\mathbf{U}$ is $M \times r$ and contains the left singular vectors of $\mathbf{A}$ and the $\mathbf{V}$ is $N \times r$ and contains the right singular vectors. The superscript H denotes complex conjugate transpose. Σ with dimensions $r \times r$ contains a diagonal matrix with r singular values of matrix $\mathbf{A}$ and the rest of its entries are zero

$$
\Sigma = \begin{bmatrix}
\sigma_1 & & & & & & \\
& \sigma_2 & & & & & \\
& & \ddots & & 0 & & \\
& & & \sigma_{r'} & & & \\
& & & & 0 & & \\
0 & & & & 0 & & \\
& & & & & \ddots & \\
& & & & & & 0
\end{bmatrix}_{r \times r}. \tag{21}
$$

The singular values below some value ε (given) are set to zero and only r' dominant singular values are retained. Since $\mathbf{U}$ and $\mathbf{V}$ are unitary matrices, we have

$$
U^{-1} = U^H \tag{22}
$$

$$
V^{-1} = V^H. \tag{23}
$$

Therefore, A^{-1} may be written as

$$
\mathbf{A}^{-1} \approx \mathbf{V}\Sigma^{-1}\mathbf{U}^{\mathbf{H}} \tag{24}
$$

where

$$
\Sigma^{-1} = \begin{bmatrix}
1/\sigma_1 & & & & 0 \\
& 1/\sigma_2 & & & \\
& & \ddots & & \\
0 & & & & \\
& & & & 1/\sigma_{r'}
\end{bmatrix}. \tag{25}
$$

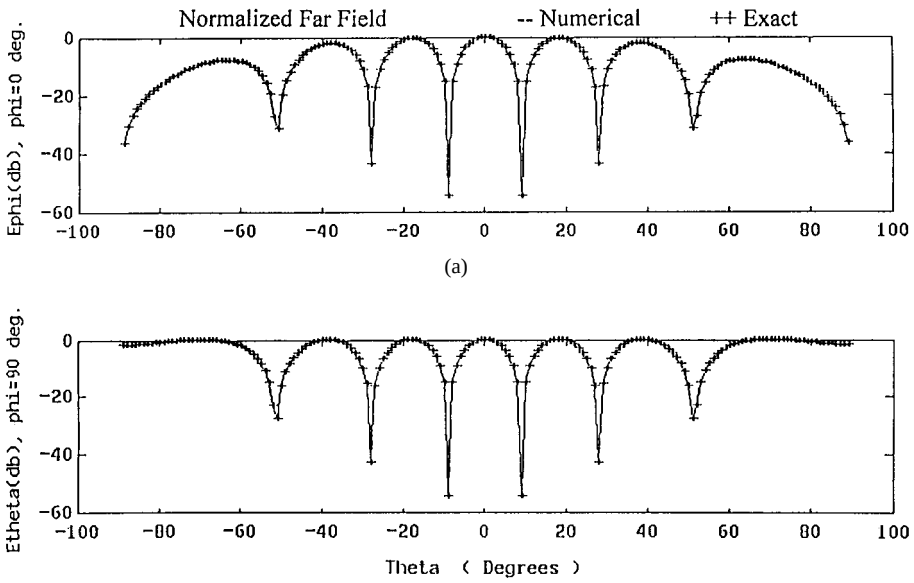

(a)

(b)

Fig. 4. (a) and (b) Comparison of exact and computed far field for $\phi = 0°$ and 90° cut for a 2 × 2 electric dipole array on a 3.6λ × 3.6λ surface. Near field was measured on an arc.

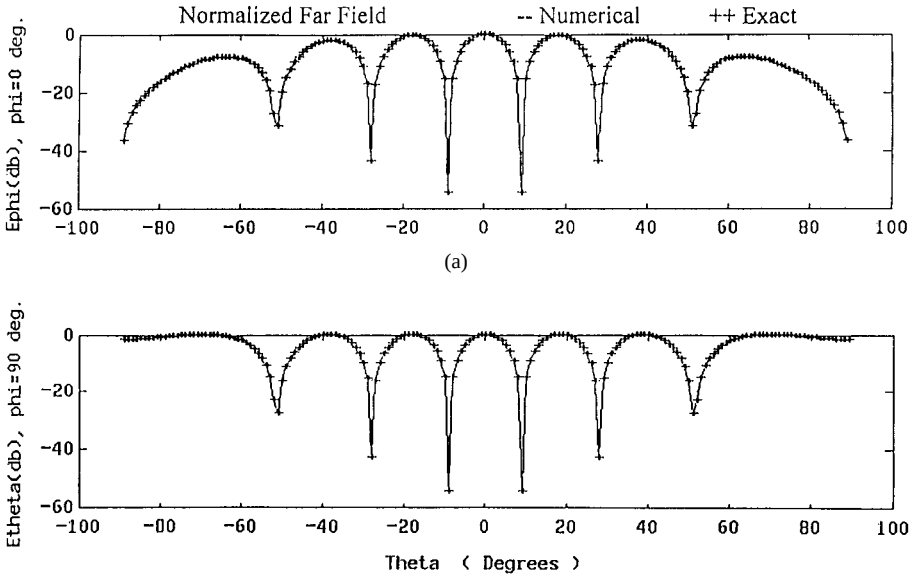

(a)

(b)

Fig. 5. (a) and (b) Comparison of exact and computed far field for $\phi = 0°$ and 90° cut for a 2 × 2 electric dipole array on a 3.6λ× 3.6λ surface. Near field was measured on a hemisphere.

Now the vector $\vec{X}$ can be determined by premultiplying $\vec{E}$ by $\mathbf{A}^{-1}$

$$\vec{X} = \mathbf{A}^{-1}\vec{\mathrm{E}}. \tag{26}$$

From (22) and (23) we have

$$\vec{X} \approx \mathbf{V}\Sigma^{-1}\mathbf{U}^{\mathbf{H}}\vec{E}. \tag{27}$$

As described by (24), the solution of the matrix equation (16) with supporting equation (17) requires no matrix inversion.

It is important to point out that the only error incurred in this theoretical procedure is truncating the surface S_∞ to S_o. How much error will this produce is still an open question. Also, the measured data need not satisfy the Nyquist sampling criteria. This sampling requirement has been transformed to the basis functions where this enforcement is quite easy.

III. Numerical Results

In this section, by the use of both synthetic and experimental near-field data, we attempt to illustrate the accuracy of the method presented here for near-field to near/far-field transformation. The results will include experiments with different antenna configurations as well as near-field data taken over various geometries. As a first example consider a four-dipole

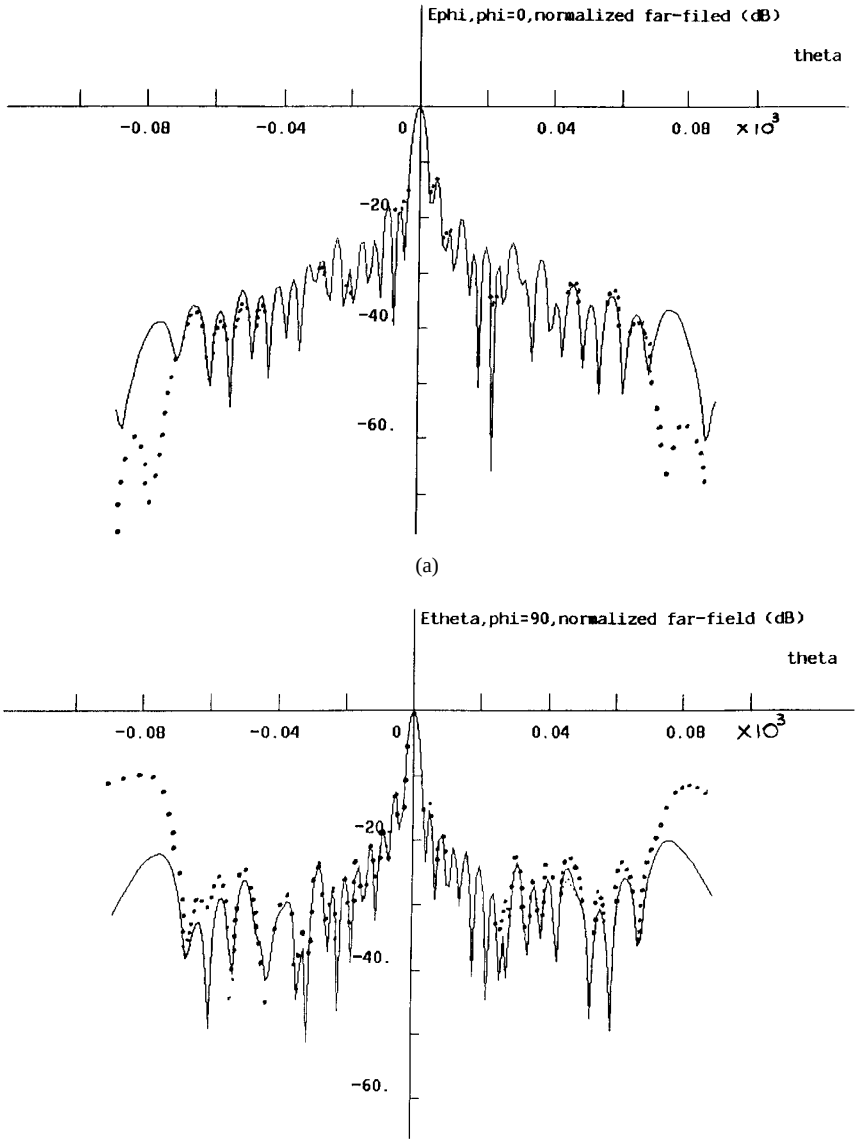

Fig. 6. Comparison of spherical modal expansion and this approach for a printed microstrip array. Measured data was used only on a hemisphere. $\cdots$ this method. _____ spherical modal expansion. (a) Comparison of the copolar plots for $\phi = 0°$. (b) comparison of the copolar plots for $\phi = 90°$.

array placed at the corners of a $3.6\lambda \times 3.6\lambda$ planar surface on the xy plane. The center of the $3.6\lambda \times 3.6\lambda$ surface is located at ($x = 0$, $y = 0$). At a spherical distance of 3λ from the origin with $0° < \theta < 30°$ and $0° < \phi < 360°$, on 200 discrete points, both the electric field components E_θ and E_ϕ are computed analytically. A fictitious planar surface in the xy plane of dimensions $4\lambda \times 4\lambda$ is used to form a planar electric current sheet. This electric current sheet is divided into 10 $\times$ 10 electric current patches. The values of these currents were determined using synthetically computed near-field data and choosing 114 singular values for the moment matrix. Fig. 4 compares the absolute value of the electric far-field components computed by the present method with the exact far field computed analytically. Fig. 4(a) presents E_ϕ in decibels for $\phi = 0°$ as a function of θ and Fig. 4(b) presents E_θ in decibels for $\phi = 90°$. The comparison is visually indistinguishable. The cross-polar components are negligible.

Next consider the same four-dipole array as described in the previous example, however, the near-field geometry is taken along an arc of a sphere. The near-field components E_θ and E_ϕ have been computed analytically along this arc with radius of 3λ and $\phi = 0°$ with $-90° < \theta < 90°$ at 1° intervals. Fig. 5(a) and (b) compares the same far fields as in Fig. 4 and again the computed and the exact results are visually indistinguishable.

Next, experimentally measured data is utilized [16]. Consider a microstrip array consisting of 32 $\times$ 32 uniformly distributed patches on a 1.5 m $\times$ 1.5 m surface. The near fields are measured at discrete points on a spherical surface at a distance 1.23 m away from the antenna at a frequency of 3.3 GHz. The data is taken every 4° in ϕ for $0° \leq \phi \leq 360°$ and every 2° in θ for $0° \leq \theta \leq 89°$, i.e., only on one hemisphere. Measurements have been performed using an open-ended cylindrical WR284 wave guide fed with TE_{11} mode. Here a fictitious planar surface on the xy plane of dimensions 1.9 m

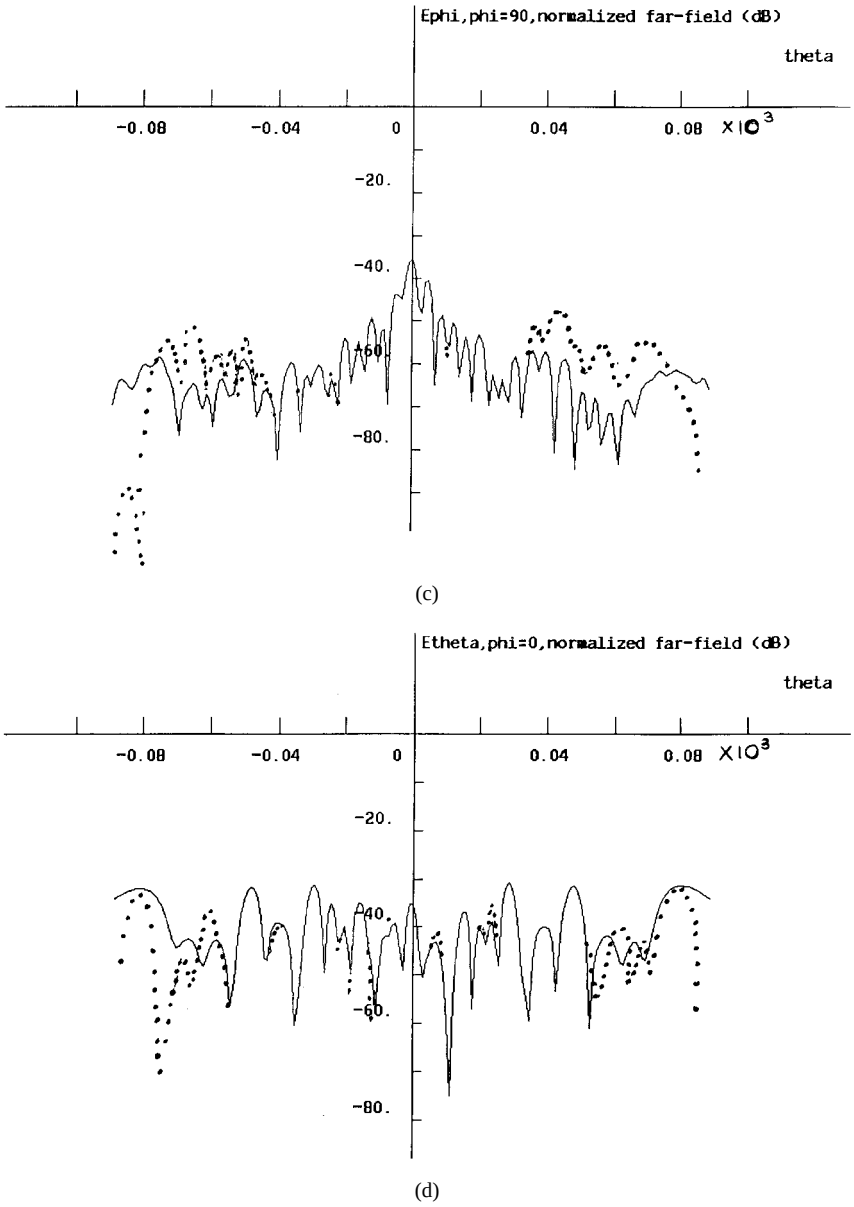

Fig. 6. (*Continued.*) Comparison of spherical modal expansion and this approach for a printed microstrip array. Measured data was used only on a hemisphere. $\cdots$ this method. —— spherical modal expansion. (c) comparison of the cross-polar plots for $\phi = 0°$. (d) comparison of the cross-polar plots for $\phi = 90°$.

$\times$ 1.9 m is used to form a electric current sheet. This electric current sheet is divided into 60 $\times$ 60 equally spaced electric current patches 0.348λ apart. The total number of unknowns for the fictitious current was 7200 as compared to the total number of field points which were 8100. The singular value cut-off in this case was 10^{-3} and the rank of the matrix was 3047. This figure compares the copolarization characteristic of the electric far-field pattern E_ϕ obtained by the present method with the result obtained numerically [16]. These numerical results are the result of near-field to far-field transformation using spherical wave expansions where the fields are expanded in terms of TM and TE to r modes. Fig. 6(a) describes $20 \log_{10} |E_\phi|$ for $\phi = 0°$ and $-89° \leq \theta \leq 89°$. Fig. 6(b) depicts the copolarization characteristic of the electric far field for $\phi = 90°$. Fig. 6(c) and (d) describes the cross-polarization characteristics of the far-field patterns. Fig. 6(c) depicts $20 \log_{10} |E_\phi|$ for $\phi = 90°$ and $-89° \leq \theta \leq 89°$.

The results are reasonable in the $-45° \leq \theta \leq 45°$ region even though the data were available from $0 \leq \theta \leq 90°$. The other curve on the figure corresponds to the spherical modal approach which utilizes the data from $0 < \theta < 180°$. It is important to note that the results obtained by the equivalent magnetic current approach [17] are more accurate than the equivalent electric current technique and it is also computationally more efficient.

IV. Conclusion

The method presented here determines the fields for $z \geq 0$ in front of the radiating antenna simply from the knowledge of the near field on any arbitrary geometry in space. Using various antenna configurations and near-field geometries, an investigation of the accuracy of this method was performed. For cases where synthetic sources were used, the far field

was compared with exact solutions and the agreements are reasonable. For cases where actual experimental sources were used, the far fields were compared with the conventional modal approach, which utilized the data from $0 < \theta < 180°$. It has been our experience that the equivalent magnetic current approach provides always a better solution than the equivalent electric current approach. This may be due to the fact that the matrix arising from the electric field operator is more ill conditioned than the matrix involved with the magnetic field operator. In addition, the fields are decoupled for the magnetic field operator [17]–[21].

ACKNOWLEDGMENT

The authors would like to thank the guest editor Dr. R. Mailloux for suggesting ways to improve the readability of the manuscript. In addition, thanks are also due to him for providing the only established, reliable, on-time mode of communication on the status of the reviews and the paper.

REFERENCES

[1] R. Laroussi and G. I. Costache, "Far-field predictions from near-field measurements using an exact integral solution," *IEEE Trans. Electromagn. Compat.*, vol. 36, pp. 189–195, Aug. 1994.
[2] J. J. H. Wang, "An examination of the theory and practices of planar near-field measurements," *IEEE Trans. Antennas Propagat.*, vol. 36, June 1988.
[3] A. J. Poggio and E. K. Miller, "Integral equation solutions of three dimensional scattering problems," in *Computer Techniques for Electromagentics*, R. Mittra, Ed. New York: Hemisphere, 1987.
[4] J. Brown and E. V. Jull, "The prediction of aerial radiation patterns from near-field measurements," *Proc. Inst. Elect. Eng.*, vol. 108B, pp. 635–644, Nov. 1961.
[5] D. M. Kerns, "Plane-wave scattering-matrix theory of antennas and antenna-antenna interactions," NBS Monograph 162, U.S. Govt. Printing Office, Washington, DC, June 1981.
[6] F. Jensen, "Electromagnetic near-field far-field correlations," Ph.D. dissertation, Tech. Univ., Copenhagen, Denmark, July 1970.
[7] P. F. Wacker, "Near-field antenna measurements using a spherical scan: Efficient data reduction with probe correction," in *Inst. Elect. Eng. Conf. Conf. Precision Electromagn. Meas.*, London, U.K., July 1974, Publ. 113, pp. 286–288.
[8] "Non-planar near-field measurements: Spherical scanning," NBSIR 75-809, June 1975.
[9] W. M. Leach and D. T. Paris, "Probe-compensated near-field measurements on a cylinder," *IEEE Trans. Antennas Propagat.*, vol. AP-21, pp. 435–445, July 1973.
[10] A. D. Yaghjian, "An overview of near-field antenna measurements," *IEEE Trans. Antennas Propagat.*, vol. AP-34, pp. 30–45, Jan. 1986.
[11] J. Appel-Hansen, "Antenna measurements," in *The Handbook of Antenna Design.* London, U.K.: Peregrinus, 1982, vol. 1, ch. 8.
[12] M. S. Narasiman and B. Preetham Kumar, "A technique of synthesizing the excitation currents of planar arrays or apertures," *IEEE Trans. Antennas Propagat.*, vol. 38, pp. 1326–1332, Sept. 1990.
[13] R. F. Harrington, *Time-Harmonic Electromagnetic Fields.* New York: McGraw-Hill, 1961.
[14] _____, *Field Computation by Moment Methods.* Orlando, FL: Krieger, 1987.
[15] G. H. Golub and C. F. Van Loan, *Matrix Computations*, 2nd ed. Baltimore, MD: Johns Hopkins Univ. Press, 1989.
[16] Spherical near-field data obtained from C. Stubenrauch, NIST, Boulder, CO.
[17] A. Taaghol and T. K. Sarkar, "Near/far field transformation for arbitarary near-field geometry utilizing an equivalent magnetic current," *IEEE Trans. Electromagn. Compat.*, vol. 38, pp. 536–542, Aug. 1996.
[18] P. Petre and T. K. Sarkar, "Planar near field to far field transformation using an equivalent magnetic current approach," *IEEE Trans. Antennas Propagat.*, vol. 40, pp. 1348–1356, Nov. 1992.
[19] _____, "Planar near field to far field transformation using an array and dipole probes," *IEEE Trans. Antennas Propagat.*, vol. 42, pp. 534–537, Apr. 1994.
[20] _____, "Difference between modal expansion and integral equation methods for planar near-field to far-field transformation," *PIER*, vol. 12, pp. 37–56, 1996.
[21] T. K. Sarkar, P. Petre, A. Taaghol, and R. F. Harrington, "An alternate spherical near-field to far-field transformation," *Progress in Electromagnetic Research.* Boston, MA: EMW, 1997, vol. 16, pp. 268–284.

Tapan Kumar Sarkar (S'69–M'76–SM'81–F'92) received the B. Tech. degree from the Indian Institute of Technology, Kharagpur, India, the M.Sc.E. degree from the University of New Brunswick, Fredericton, Canada, the M.S. and Ph.D. degrees from Syracuse University, Syracuse, NY, in 1969, 1971, and 1975, respectively, and the Docteur Honoris Causa from the Universite of Blaise Pascal at Clermont-Ferrand, France, in 1998.

From 1975 to 1976, he was with the TACO Division, General Instruments Corporation. From 1976 to 1985 he was with the Rochester Institute of Technology, Rochester, NY. From 1977 to 1978 he was a Research Fellow at the Gordon McKay Laboratory, Harvard University, Cambridge, MA. He is now a Professor in the Department of Electrical and Computer Engineering, Syracuse University. He has authored or coauthored more than 188 journal articles and has ten books. He is currently on the editorial board of JEWA and MIT. His current research interests deal with numerical solutions of operator equations arising in electromagnetics and signal processing with application to system design which includes analysis of signal integrity in high speed computer systems and real-time adaptive processing for mobile wireless systems.

Dr. Sarkar is a registered Professional Engineer in New York State. He was an associate editor for feature articles of the *IEEE Antennas and Propagation Society Newsletter* and was the Technical Program Chairman for the 1988 IEEE Antennas and Propagation Society International Symposium and the URSI Radio Science Meeting. He was the Chairman of the Intercommission Working Group of International URSI on time domain metrology. He is a member of Sigma Xi and the International Union of Radio Science Commissions A and B. He received one of the "Best Solution" Awards in May 1977 at the Rome Air Development Center (RADC) Spectral Estimation Workshop, Rome, NY. He received the Best Paper Award of the IEEE TRANSACTIONS ON ELECTROMAGNETIC COMPATIBILITY in 1979 and in the 1997 National Radar Conference.

Ardalan Taaghol, photograph and biography not available at the time of publication.